

# Detection of Orbital Fluctuations Above the Structural Transition Temperature in the Iron Pnictides and Chalcogenides

H. Z. Arham<sup>1</sup>, C. R. Hunt<sup>1</sup>, W. K. Park<sup>1</sup>, J. Gillett<sup>2</sup>, S. D. Das<sup>2</sup>, S. E. Sebastian<sup>2</sup>, Z. J. Xu<sup>3</sup>, J. S. Wen<sup>3</sup>, Z. W. Lin<sup>3</sup>, Q. Li<sup>3</sup>, G. Gu<sup>3</sup>, A. Thaler<sup>4</sup>, S. Ran<sup>4</sup>, S. L. Bud'ko<sup>4</sup>, P. C. Canfield<sup>4</sup>, D. Y. Chung<sup>5</sup>, M. G. Kanatzidis<sup>5</sup>, L. H. Greene<sup>1</sup>

<sup>1</sup>*Department of Physics and the Frederick Seitz Material Research Laboratory, University of Illinois at Urbana-Champaign, Urbana, Illinois 61801, USA*

<sup>2</sup>*Cavendish Laboratory, J. J. Thomson Ave, University of Cambridge, UK*

<sup>3</sup>*Condensed Matter Physics and Materials Science Department, Brookhaven National Laboratory, Upton, New York, 11973, USA*

<sup>4</sup>*Ames Laboratory & Department of Physics and Astronomy, Iowa State University, Ames, IA, 50011, USA*

<sup>5</sup>*Materials Science Division, Argonne National Laboratory, Argonne, IL 60439, USA*

(Dated: May 29, 2022)

We use point contact spectroscopy to probe  $\text{AEFe}_2\text{As}_2$  ( $\text{AE} = \text{Ca}, \text{Sr}, \text{Ba}$ ) and  $\text{Fe}_{1+y}\text{Te}$ . For  $\text{AE} = \text{Sr}, \text{Ba}$  we detect orbital fluctuations above  $T_S$  while for  $\text{AE} = \text{Ca}$  these fluctuations start below  $T_S$ . Co doping preserves the orbital fluctuations while K doping suppresses it. The fluctuations are only seen at those dopings and temperatures where an in-plane resistive anisotropy is known to exist. We predict an in-plane resistive anisotropy of  $\text{Fe}_{1+y}\text{Te}$  above  $T_S$ . Our data are examined in light of the recent work by W.-C. Lee and P. Phillips (arXiv:1110.5917v1).

The parent compounds of the iron based superconductors undergo a  $C_4$  symmetry breaking transition when entering an antiferromagnetic orthorhombic ground state [1–6]. It is not clear if this transition is driven by magnetic fluctuations [7, 8] or orbital ordering [9–12]. There is evidence that the quantum critical fluctuations associated with this transition are nematic in character and extend into the normal state of these compounds [13, 14].

Point contact spectroscopy (PCS) measures the differential conductance  $dI/dV = G(V)$  of a ballistic junction comprised of two metals, N and M.  $G(V)$  shows the propensity of M to either reflect or absorb the quasiparticles injected into it from N. An energy dependent density of states (DOS) for M is therefore reflected in  $G(V)$ . Any excitation mode capable of scattering the injected electrons also affects  $G(V)$ . Thus PCS provides a direct picture of the electronic structure of M. If M is a superconductor, PCS detects Andreev reflection [15], and  $G(V)$  contains information on the superconducting order parameter magnitude and symmetry. For heavy fermion compounds, the onset of the Kondo lattice appears as a Fano lineshape in PCS spectra [16].

PCS results reported on the Fe-based compounds thus far focus on their superconducting (S) phase [17]. In this study, we use PCS to probe the following compounds at both S and non-S dopings and temperatures:  $\text{AEFe}_2\text{As}_2$  ( $\text{AE} = \text{Ca}, \text{Sr}, \text{Ba}$ ),  $\text{Ba}(\text{Fe}_{1-x}\text{Co}_x)_2\text{As}_2$ ,  $\text{Ba}_{0.8}\text{K}_{0.2}\text{Fe}_2\text{As}_2$  and  $\text{Fe}_{1+y}\text{Te}$ . For  $\text{Fe}_{1+y}\text{Te}$ ,  $\text{SrFe}_2\text{As}_2$  and underdoped  $\text{Ba}(\text{Fe}_{1-x}\text{Co}_x)_2\text{As}_2$  we detect a conductance enhancement well above the magnetic ( $T_N$ ) and structural ( $T_S$ ) transition temperatures; for  $\text{CaFe}_2\text{As}_2$  this enhancement is only observed below  $T_N$  and  $T_S$  while it is not observed at all for  $\text{Ba}_{0.8}\text{K}_{0.2}\text{Fe}_2\text{As}_2$  and overdoped  $\text{Ba}(\text{Fe}_{1-x}\text{Co}_x)_2\text{As}_2$ . We relate the  $dI/dV$  spectrum to the non-Fermi liquid behavior in these compounds that is manifested as an in-plane resistivity anisotropy, which

has been attributed to orbital fluctuations [18].

Single crystals of  $\text{SrFe}_2\text{As}_2$  and  $\text{Ba}(\text{Fe}_{1-x}\text{Co}_x)_2\text{As}_2$  are grown out of FeAs flux as described in [19, 20] (for  $x=0$  to 0.08) and [21] (for  $x=0.085$  to 0.125).  $\text{CaFe}_2\text{As}_2$  crystals are grown from both Sn and FeAs flux [22], while  $\text{Ba}_{0.8}\text{K}_{0.2}\text{Fe}_2\text{As}_2$  crystals are grown in Sn flux [23].  $\text{Fe}_{1+y}\text{Te}$  single crystals are grown by a horizontal unidirectional solidification method [24]. Metallic junctions are formed on freshly cleaved c-axis crystal surfaces and  $G(V)$  across each junction is measured using a standard four-probe lock-in technique. PCS is carried out in two different configurations: the needle-anvil method and the soft PCS method [17, 25]. In the needle-anvil setup, an electrochemically polished Au tip is brought into gentle contact with the sample. For soft PCS, we sputter 50Å  $\text{AlO}_x$  on our crystals to act as an insulating barrier. Using Ag paint as a counter electrode, parallel, nanoscale channels are introduced for ballistic current transport by fritting [26] across the oxide layer. Similar spectra are obtained from both methods. Raw  $G(V)$  data obtained via soft PCS are presented here.

Fig. 1a shows  $G(V)$  for  $\text{BaFe}_2\text{As}_2$  ( $T_N = T_S \sim 132$  K, slightly lower than the 134 K reported in literature [21]). At the lowest temperature (blue curve), we see a dip at zero bias and two asymmetric conductance peaks at  $\sim 65$  mV. This double peak feature is superimposed on a parabolic background. As the temperature is increased, the dip at zero bias fills, the conductance peaks move inward, and the bias voltage range of the conductance enhancement decreases. No dramatic change in the spectra is observed as  $T_S$  is crossed (red curve). The enhancement eventually disappears leaving behind the parabolic background at 177 K, more than 40 K above  $T_S$ . We define  $T_o$  as the temperature below which the conductance enhancement is observed. Similar spectra are obtained from two other underdoped non-S samples:

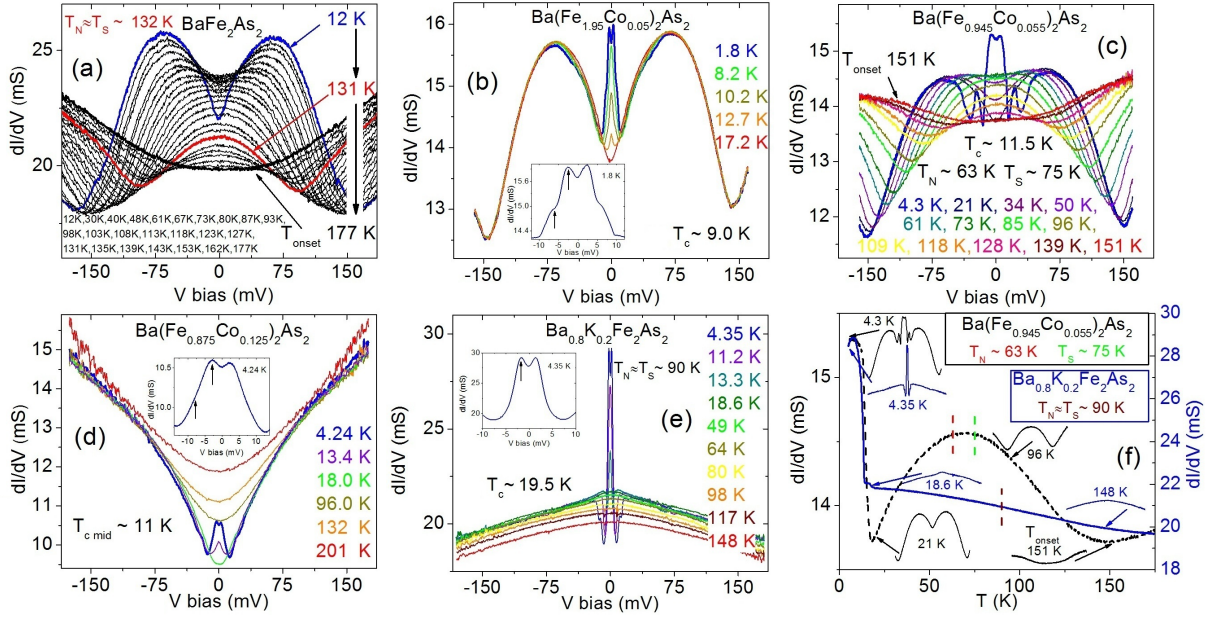


FIG. 1. (a) Conductance spectra for  $\text{BaFe}_2\text{As}_2$ . Conductance enhancement with peaks at  $\sim 65\text{mV}$  superimposed on a parabolic background is observed at low temperatures. The peaks move in as the temperature is increased and the enhancement survives well above  $T_S$  (red curve) (b, c)  $\text{Ba}(\text{Fe}_{0.95}\text{Co}_{0.05})_2\text{As}_2$  and  $\text{Ba}(\text{Fe}_{0.945}\text{Co}_{0.055})_2\text{As}_2$  display a coexistence of magnetism and superconductivity. At low temperatures, clear Andreev peaks are observed (inset Figure 1b, the arrows are pointing out the Andreev peaks). A conductance enhancement with peaks at  $\sim 65\text{mV}$  coexists with the Andreev spectra and evolves with temperature as it does for  $\text{BaFe}_2\text{As}_2$ . (d) The overdoped compound  $\text{Ba}(\text{Fe}_{0.875}\text{Co}_{0.125})_2\text{As}_2$  shows Andreev spectra below  $T_c$ . It does not have conductance peaks at higher bias values like the Co underdoped compounds. (e) The hole doped  $\text{Ba}_{0.8}\text{K}_{0.2}\text{Fe}_2\text{As}_2$  has a coexistence of superconductivity and magnetism. It shows Andreev spectra below  $T_c$  and no higher bias conductance enhancement. (f) The zero bias conductance (ZBC) vs. temperature curves for  $\text{Ba}(\text{Fe}_{0.945}\text{Co}_{0.055})_2\text{As}_2$  and  $\text{Ba}_{0.8}\text{K}_{0.2}\text{Fe}_2\text{As}_2$  corresponding to Figures 1c and e. Both compounds have a magnetostructural transition and a superconducting transition. Co doping shows a conductance enhancement that survives beyond  $T_S$  while K doping does not. The insets correlate the spectra obtained at different temperatures to the ZBC curves.

$x=0.015$  ( $T_S \sim 119\text{ K}$ ,  $T_o \sim 165\text{ K}$ ); and  $x=0.025$  ( $T_S \sim 107\text{ K}$ ,  $T_o \sim 160\text{ K}$ ). For Co underdoped samples  $T_N < T_S$ .

Fig. 1b shows  $G(V)$  for  $x=0.05$ , where long-range magnetic order coexists with superconductivity ( $T_c=9.0\text{ K}$ ,  $T_S \sim 78\text{ K}$ ). At  $1.8\text{ K}$ , the lower bias voltages ( $< 15\text{ mV}$ ) are dominated by Andreev reflection (Fig. 1b inset). However, just like the parent compound, two conductance peaks occur at  $\sim 65\text{ mV}$ . As the temperature is increased, Andreev reflection dies out and the high bias conductance evolves just like it does for  $\text{BaFe}_2\text{As}_2$ . Fig. 1c shows  $G(V)$  for another coexisting sample  $x=0.055$  ( $T_c=11.5\text{ K}$ ,  $T_S \sim 75\text{ K}$ ) depicting the same features. The split Andreev peaks at low temperature attest to the good quality of our junctions [17]. The high-bias conductance features are completely reproducible, and coexist with the clean Andreev signal, indicating they are not experimental artifacts.

Fig. 1d shows  $G(V)$  for an overdoped sample with  $x=0.125$  ( $T_c=11\text{ K}$ , no  $T_S$ ). At  $4.5\text{ K}$ , superconducting Andreev peaks are observed (Fig. 1d inset). Unlike the underdoped samples, no high bias conductance peaks are observed. Above the superconducting transition only a V-shaped background remains. Near optimally doped

samples with  $x=0.07$  ( $T_c=22\text{ K}$ ) and  $x=0.08$  ( $T_c=24\text{ K}$ ) show similar spectra with Andreev peaks below  $T_c$  and a V-shaped background above it (data not shown).

Fig. 1e shows  $G(V)$  for  $\text{Ba}_{0.8}\text{K}_{0.2}\text{Fe}_2\text{As}_2$ . The sample shows a coexistence of magnetism and superconductivity [27] ( $T_N=T_S \sim 90\text{ K}$ ,  $T_c \sim 20\text{ K}$ ). Low temperature spectra show Andreev peaks (Fig. 1e inset). The Andreev signal disappears at  $\sim 15\text{ K}$  leaving behind a background that does not change with a further increase in temperature.

Fig. 1f shows zero bias conductance (ZBC) curves for  $\text{Ba}(\text{Fe}_{0.945}\text{Co}_{0.055})_2\text{As}_2$  and  $\text{Ba}_{0.8}\text{K}_{0.2}\text{Fe}_2\text{As}_2$ . Superconductivity and magnetism coexist in both samples and both show Andreev spectra below  $T_c$ . However, while Co doping shows a conductance enhancement that lasts above  $T_S$ , no such enhancement is observed for K doping.

Fig. 2a shows the  $G(V)$  for  $\text{SrFe}_2\text{As}_2$  and Fig. 2b for  $\text{CaFe}_2\text{As}_2$ . The trend for  $\text{SrFe}_2\text{As}_2$  is very similar to that of  $\text{BaFe}_2\text{As}_2$ . It has a  $T_N=T_S$  of  $\sim 190\text{ K}$  and a  $T_o$  of  $\sim 240\text{ K}$ . (Data are taken on an unannealed sample, annealing increases  $T_S$  to  $200\text{ K}$  [20]). However,  $\text{CaFe}_2\text{As}_2$  shows a different behavior. Of the 13 junctions tested, 11 of them showed a conductance enhancement disappearing around  $100\text{ K}-110\text{ K}$ , below  $T_N=T_S \sim 170\text{ K}$ .

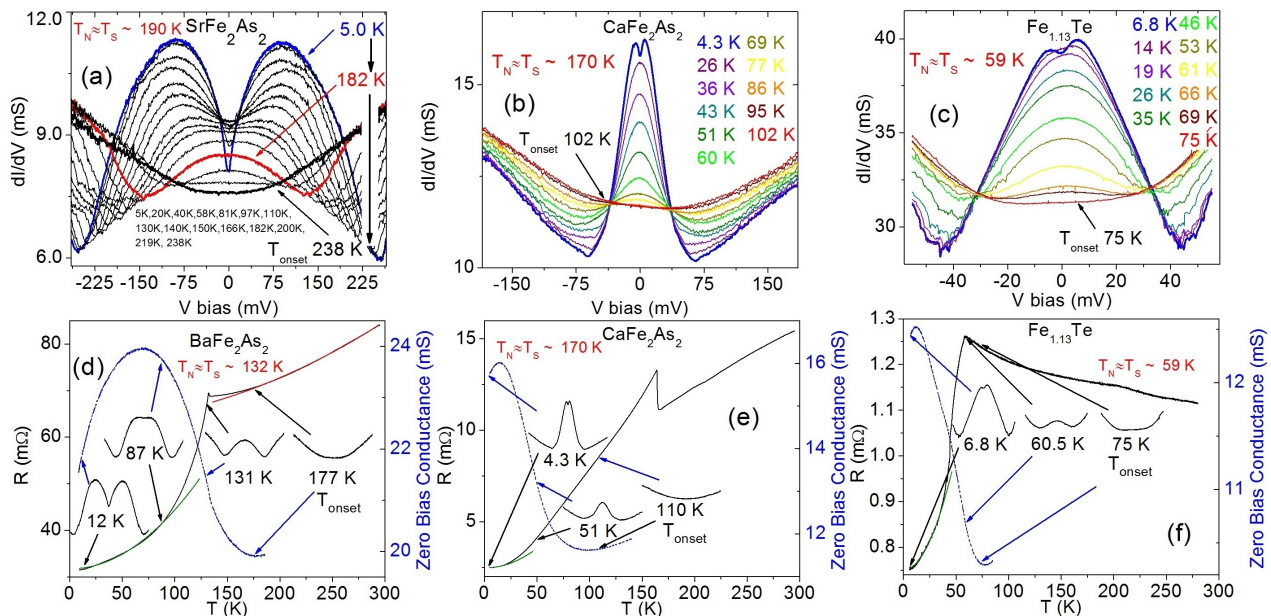


FIG. 2. (a) Conductance spectra for  $\text{SrFe}_2\text{As}_2$ . The conductance enhancement lasts above  $T_S$  and the spectra is similar to that of  $\text{BaFe}_2\text{As}_2$  (Figure 1a). (b) Conductance spectra for  $\text{CaFe}_2\text{As}_2$ . In this case the conductance enhancement disappears before  $T_S$ . (c) Conductance spectra for  $\text{Fe}_{1.13}\text{Te}$  shows an enhancement that lasts above  $T_S$ . (d-f) The ZBC and the resistance vs. temperature,  $R(T)$ , curves for  $\text{BaFe}_2\text{As}_2$ ,  $\text{CaFe}_2\text{As}_2$  and  $\text{Fe}_{1.13}\text{Te}$ . For  $\text{CaFe}_2\text{As}_2$  the enhancement disappears before  $T_S$  while for  $\text{BaFe}_2\text{As}_2$  and  $\text{Fe}_{1.13}\text{Te}$  it lasts into the normal state. The insets correlate the spectra obtained at different temperatures to the ZBC curve. The red and green curves are fits to  $\rho = \rho_0 + AT^2$ .

For the remaining 2, the enhancement is observed till 170-180K. Fig. 2c shows  $G(V)$  for the Fe-chalcogenide  $\text{Fe}_{1.13}\text{Te}$ . The conductance enhancement is observed till 75 K ( $T_N = T_S \sim 59$  K).  $\text{Fe}_{1.03}\text{Te}$  shows a conductance enhancement that lasts till 85 K ( $T_N = T_S \sim 69$  K).

Figs. 2d-f show ZBC and  $R(T)$  curves for  $\text{BaFe}_2\text{As}_2$ ,  $\text{CaFe}_2\text{As}_2$  and  $\text{Fe}_{1.13}\text{Te}$ . The curves clearly show the enhancement lasting well above  $T_S$  for  $\text{BaFe}_2\text{As}_2$  and  $\text{Fe}_{1.13}\text{Te}$ , and disappearing before  $T_S$  for  $\text{CaFe}_2\text{As}_2$ . The insets in the figure correlate the spectra obtained at different temperatures to the ZBC and  $R(T)$  curves.

The Fe-pnictides and the Fe-chalcogenides show very different resistivity curves and may be classified as bad metals [28]. Upon cooling the  $\text{Fe}_{1.13}\text{Te}$  from room temperature to  $T_S$ , the resistance is observed to increase, while for the  $\text{BaFe}_2\text{As}_2$ , the resistance is seen to decrease. Below  $T_S$ , the resistance decreases much more quickly with decreasing temperature for  $\text{Fe}_{1.13}\text{Te}$  than for  $\text{BaFe}_2\text{As}_2$ . Despite differences in their  $R(T)$ , the two families show similarly shaped  $G(V)$  spectra. This indicates that our observed conductance feature cannot be accounted for by local heating effect, and our junctions are either in the ballistic or diffusive regimes [17, 25]. In the thermal regime, the junction resistance depends on the bulk resistivity of the crystals, and different shaped spectra for  $\text{BaFe}_2\text{As}_2$  and  $\text{Fe}_{1.13}\text{Te}$  would be seen.

To summarize thus far, we have studied Fe-based compounds that exhibit a magnetostructural transition.

$\text{BaFe}_2\text{As}_2$ ,  $\text{SrFe}_2\text{As}_2$ , underdoped  $\text{Ba}(\text{Fe}_{1-x}\text{Co}_x)_2\text{As}_2$  and  $\text{Fe}_{1+y}\text{Te}$  exhibit a  $dI/dV$  enhancement that sets in above  $T_S$ ,  $\text{CaFe}_2\text{As}_2$  only shows the enhancement below  $T_S$  while  $\text{Ba}_{0.8}\text{K}_{0.2}\text{Fe}_2\text{As}_2$  does not show any conductance enhancement. Overdoped  $\text{Ba}(\text{Fe}_{1-x}\text{Co}_x)_2\text{As}_2$  does not have a  $T_S$  and only shows Andreev spectra below  $T_c$ .

We compare the presence of the conductance enhancement with the in-plane resistivity behavior of these compounds. For detwinned underdoped  $\text{AEFe}_2\text{As}_2$  it has been shown that below  $T_S$  a resistive anisotropy exists [29, 30]. Above  $T_S$  there is notable anisotropy for  $\text{AE}=\text{Ba}$ , negligible anisotropy for  $\text{AE}=\text{Sr}$  and no anisotropy for  $\text{AE}=\text{Ca}$  (Figure 5 in [30]). The anisotropy above  $T_S$  is sensitive to the uniaxial force required to detwin the samples. Detwinned underdoped  $\text{Ba}_{1-x}\text{K}_x\text{Fe}_2\text{As}_2$  does not show any anisotropy at all, either below or above  $T_S$  [31]. In this work we use PCS to probe twinned samples along the  $c$ -axis. The presence or absence of the in-plane resistive anisotropy matches with whether a conductance enhancement is detected or not. This indicates that the conductance enhancement we observe is caused by the same phenomenon that causes the in-plane resistive anisotropy in these compounds. Due to inherent difficulties in detwinning  $\text{Fe}_{1+y}\text{Te}$ , it has not been tested for resistive anisotropy, but since we observe conductance enhancement above  $T_S$ , we expect it to have a resistive anisotropy that sets in above  $T_S$ .

The normal state resistivity of metals may be fit to a

power law  $\rho = \rho_0 + AT^\alpha$  where  $\alpha=2$  for standard Fermi liquid theory. Fig. 2d shows such a fit for twinned  $\text{BaFe}_2\text{As}_2$ . From 300 K down to  $\sim 180$  K, the resistance follows a  $T^2$  dependence ( $R^2$  for fit is 0.9998). The deviation from  $\alpha=2$  sets in very close to  $T_o$ . This suggests that the conductance enhancement observed by PCS is tied to the deviation from Fermi liquid behavior in  $\text{BaFe}_2\text{As}_2$ . For near optimal doping,  $\alpha \approx 1$ , and with increasing doping, increases back towards 2 for overdoped crystals.

We construct a revised phase diagram for  $\text{Ba}(\text{Fe}_{1-x}\text{Co}_x)_2\text{As}_2$ , (Fig. 3a) marking a new line on the underdoped side showing the temperature below which the conductance enhancement is observed.

Recent work [18] has shown that orbital fluctuations above  $T_S$  are expected to provide extra contributions to the single particle DOS at zero energy. The DOS follow a log dependence as the energy is increased. Fig. 3b shows that our conductance enhancement for  $\text{BaFe}_2\text{As}_2$  above  $T_S$  follows a log dependence from  $\sim 40$  mV to  $\sim 90$  mV. Thermal population effects at 135 K causes scatter in the data at low bias voltage. Similar fits are observed above  $T_S$  for  $\text{SrFe}_2\text{As}_2$  and  $\text{Fe}_{1.13}\text{Te}$ . Furthermore, the absence of similar effects in our data on  $\text{Ba}_{0.8}\text{K}_{0.2}\text{Fe}_2\text{As}_2$  is consistent with the prediction that crystals that do not show the resistance anisotropy will also not exhibit the excess conductance due to orbital fluctuations [18]. Our data therefore strongly indicates that the enhancement in conductance observed by our experiments is a consequence of orbital fluctuations.

Note that with decreasing temperature, the excess conductance curves all develop a dip at zero bias that sharpens as the temperature is lowered further (most clearly seen in in Fig. 1a). Similarly shaped PCS  $dI/dV$  curves are obtained in dilute Kondo alloys, accounted for by the interference of the Kondo scattered and conduction electrons [25]. Our conductance curves can be similarly accounted for by orbital ordering: Here, the two interfering channels are the nearly-degenerate  $d_{zx}$  and  $d_{zy}$  orbitals, and this now is entirely consistent with the log dependence of the conductance shown in Fig. 3b and discussed above [18]. It is also worth noting that this shape is not reminiscent of a gap: The split peaks observed from Andreev reflection are concave upward at zero bias.

For the  $\text{BaFe}_2\text{As}_2$  sample in Fig. 2d, the temperature at which  $G(V)$  develops a dip at zero bias ( $\sim 90$  K) is the same temperature at which the resistance again moves towards a  $T^2$  dependence. A similar trend may be pointed out for  $\text{CaFe}_2\text{As}_2$  and  $\text{Fe}_{1.13}\text{Te}$  (Green curves in Fig. 2e, f). The  $T^2$  fit is heuristic in nature as it ignores magnon/phonon contribution to the resistivity.

A maximum is observed at  $\sim 200$ K in the interplane c-axis resistivity of  $\text{BaFe}_2\text{As}_2$  [32], marking the crossover from high temperature nonmetallic to low temperature metallic behavior. Upon Co doping, the maximum moves to a lower temperature. The  $T_o$  determined from our PCS data occurs at a comparable temperature to this

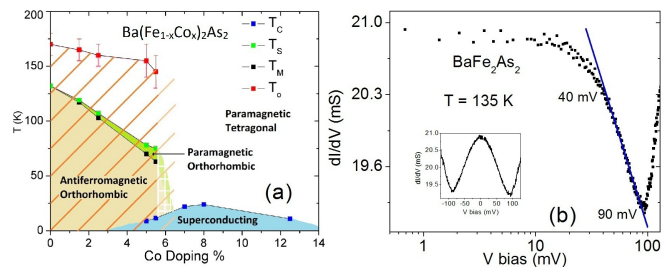


FIG. 3. (a) Phase diagram for  $\text{Ba}(\text{Fe}_{1-x}\text{Co}_x)_2\text{As}_2$ . For the underdoped side, a new region is marked (diagonal stripes) indicating the conductance enhancement that sets in above  $T_S$ . (b)  $G(V)$  above  $T_S$  for  $\text{BaFe}_2\text{As}_2$  follows a log dependence from  $\sim 40$  mV to  $\sim 90$  mV.

maximum. However, we only observe  $T_o$  for Co underdoped samples, while the c-axis resistivity maximum exists throughout the overdoped region.

Evidence for normal state nematicity from detwinned samples is complicated by the symmetry breaking pressure applied to detwin the crystal. Apart from the resistive anisotropy already discussed, ARPES [33] detects orbital ordering, and optical conductivity [34] an in-plane anisotropy in the normal state. On twinned samples, inelastic neutron scattering reveals high energy ( $>100$ meV) spin excitations above  $T_S$  in  $\text{BaFe}_2\text{As}_2$  [14], although that these are truly indicative of nematicity is controversial [35], and torque magnetometry on  $\text{BaFe}_2(\text{As}_{1-x}\text{P}_x)_2$  detects a  $C_4$  symmetry breaking in the normal state, across the phase diagram [36].

In conclusion, we have performed PCS measurements on twinned  $\text{AEFe}_2\text{As}_2$  ( $\text{AE}=\text{Ca}, \text{Sr}, \text{Ba}$ ),  $\text{Ba}(\text{Fe}_{1-x}\text{Co}_x)_2\text{As}_2$ ,  $\text{Ba}_{0.8}\text{K}_{0.2}\text{Fe}_2\text{As}_2$  and  $\text{Fe}_{1+y}\text{Te}$ . We observe a conductance enhancement which is indicated to arise from orbital fluctuations that increase the single particle DOS at zero energy [18]. The enhancement sets in above  $T_S$  for those compounds that are known to exhibit an in-plane resistive anisotropy above  $T_S$ . Based on the data from our PCS experiments, therefore, an in-plane resistive anisotropy of untwinned  $\text{Fe}_{1+y}\text{Te}$  that onsets above  $T_S$  is anticipated. Our experiments provide support for orbital nematicity in  $\text{BaFe}_2\text{As}_2$ ,  $\text{SrFe}_2\text{As}_2$  and  $\text{Fe}_{1+y}\text{Te}$ .

We thank P. Phillips and W.-C. Lee for valuable and motivating discussions. We also thank N. Ni for sharing resistance data for  $\text{Ba}(\text{Fe}_{1-x}\text{Co}_x)_2\text{As}_2$ . This work is supported as part of the Center for Emergent Superconductivity, an Energy Frontier Research Center funded by the US Department of Energy, Office of Science, Office of Basic Energy Sciences under Award No. DE-AC0298CH1088. Ames Lab is operated by ISU under DOE Contract No. DE-AC02-07CH11358. University of Cambridge is supported by EPSRC, Trinity College, the Royal Society and the Commonwealth Trust.

- 
- [1] C. de la Cruz *et al.*, Nature **453**, 899 (2008).
- [2] M. Rotter *et al.*, Phys. Rev. B **78**, 020503 (2008).
- [3] C. Lester *et al.*, Phys. Rev. B **79**, 144523 (2009).
- [4] D. K. Pratt *et al.*, Phys. Rev. Lett. **103**, 087001 (2009).
- [5] W. Bao *et al.*, Phys. Rev. Lett. **102**, 247001 (2009).
- [6] N. Ni *et al.*, Phys. Rev. B **78**, 014523 (2008).
- [7] C. Fang *et al.*, Phys. Rev. B **77**, 224509 (2008).
- [8] T. Yildirim *et al.*, Phys. Rev. Lett. **102**, 037003 (2009).
- [9] F. Kruger *et al.*, Phys. Rev. B **79**, 054504 (2009).
- [10] C.-C. Chen *et al.*, Phys. Rev. B **80**, 180418 (2009); **82**, 100504(R) (2010).
- [11] W. Lv *et al.*, Phys. Rev. B **80**, 224506 (2009); **82**, 045125 (2010).
- [12] C.-C. Lee *et al.*, Phys. Rev. Lett. **103**, 267001 (2009).
- [13] J.-H. Chu *et al.*, Science **329**, 824 (2010).
- [14] L. W. Harriger *et al.*, Phys. Rev. B **84**, 054544 (2011).
- [15] A. F. Andreev. *et al.*, Sov. Phys. JETP **19**, 1228 (1964).
- [16] W. K. Park *et al.*, Phys. Rev. Lett. **100**, 177001 (2008).
- [17] D. Daghero *et al.*, Super. Sci. Tech. **23**, 043001 (2010); Rep. Prog. Phys. **74**, 124509 (2011).
- [18] W.-C. Lee *et al.*, arXiv:1110.5917v1.
- [19] S. E. Sebastian *et al.*, J. Phys.: Cond. Matt. **20**, 422203 (2008).
- [20] J. Gillett *et al.*, arXiv:1005.1330v1.
- [21] N. Ni *et al.*, Phys. Rev. B **78**, 214515 (2008).
- [22] S. Ran *et al.*, Phys. Rev. B **83**, 144517 (2011).
- [23] D. Y. Chung *et al.*, unpublished.
- [24] J. Wen *et al.*, Rep. Prog. Phys. **74**, 124503 (2011).
- [25] Y. G. Naidyuk and I. K. Yanson, 2005 Point-Contact Spectroscopy (New York: Springer).
- [26] R. Holm, 1958 Electric Contacts Handbook (Berlin: Springer).
- [27] S. Avci *et al.*, Phys. Rev. B **83**, 172503 (2011).
- [28] D. C. Johnston, Advances in Physics **59**, 803 (2010).
- [29] M. A. Tanatar *et al.*, Phys. Rev. B **81**, 184508 (2010).
- [30] E. C. Blomberg *et al.*, Phys. Rev. B **83**, 134505 (2011).
- [31] J. J. Ying *et al.*, Phys. Rev. Lett. **107**, 067001 (2011).
- [32] M. A. Tanatar *et al.*, Phys. Rev. B **82**, 134528 (2010).
- [33] M. Yi *et al.*, PNAS **108**, 6878 (2011).
- [34] A. Dusza *et al.*, EPL **93**, 37002 (2011).
- [35] H. Park *et al.*, Phys. Rev. Lett. **107**, 137007 (2011).
- [36] Private communication with Y. Matsuda; S. Kashahara *et al.*, Bull. Am. Phys. Soc. **56**, Z26.00010 (2011).